MEASUREMENT OF PHOTOEMISSION AND SECONDARY EMISSION FROM LABORATORY DUST GRAINS

Final Report

Robert C. Hazelton, Edward J. Yadlowsky
Thomas B. Settersten, Gregory G. Spanjers, and John J. Moschella
HY-Tech Research Corporation
104 Centre Court
Radford, VA 24141
(540) 639-4019

Based on work performed under

Contract NASW-4600

July 21, 1995

MEASUREMENT OF PHOTOEMISSION AND SECONDARY EMISSION FROM LABORATORY DUST GRAINS

Abstract

The overall goal of this project is experimentally determine the emission properties of dust grains in order to provide theorists and modelers with an accurate data base to use in codes that predict the charging of grains in various plasma environments encountered in the magnetospheres of the planets. In general these modelers use values which have been measured on planar, bulk samples of the materials in question. The large enhancements expected due to the small size of grains can have a dramatic impact upon the predictions and the ultimate utility of these predictions.

The first experimental measurement of energy resolved profiles of the secondary electron emission coefficient, δ, of sub-micron diameter particles has been accomplished. Bismuth particles in the size range of .022 to .165 μm were generated in a moderate pressure vacuum oven (average size is a function of oven temperature and pressure) and introduced into a high vacuum chamber where they interacted with a high energy electron beam (0.4 to 20 keV). Large enhancements in emission were observed with a peak value, $\delta_{max} = 4.5$ measured for the ensemble of particles with a mean size of .022 μm. This is in contrast to the published value, $\delta_{max} = 1.2$, for bulk bismuth. The observed profiles are in general agreement with recent theoretical predictions made by Chow et al. at UCSD.

I. INTRODUCTION

Dust grains and plasmas are commingled in many places in the universe ranging from interstellar space to earth bound manufacturing processes. Examples of space born dusty plasmas range from protostellar clouds [1-3] to planetary rings [4-6] to cometary tails [7-9] to the earth's magnetosphere [10,11]. Examples of earth bound dusty plasmas range from plasma spray systems [12], to contaminating particulates in semiconductor plasma processors [13-16], to pollutant particles in electrostatic precipitators [17-19]. The ramifications of the plasma/grain interactions are unique to each of the systems mentioned. For example, the accretion or segregation of particles in a protostellar cloud may depend strongly on the net charge accumulated on grains of different sizes and compositions. Oppositely charged particles could lead to an accretion of grains while similarly charged particles could prevent accretion and particle growth [1]. As an example, it has been postulated that grain charging events can account for the spokes observed in planetary rings and out of plane dust eruptions [6].

In the case of earth bound plasmas, powders are the feedstock for plasma spray units and an understanding of the interactions of grains and plasmas are important [12]. In electrostatic precipitators it is essential that a charge be transferred to pollutant particles to allow electric fields to draw the grains out of the background gas [19]. Finally, recent studies have shown that plasma processing tools used in the manufacture of semiconductors can generate dust particles which become trapped in the plasma and can subsequently deposit them on the wafer surfaces[13]. As feature sizes are reduced in the coming years, the importance of controlling contaminating dust will become even more significant.

A great deal of effort has gone into the modeling of dust/plasma interactions [20-24], and some experimental work has recently been initiated to study such interactions [25,26]. Experimental studies are needed for a number of reasons. First of all, one must experimentally determine many of the parameters such as secondary electron emission or photoemission coefficients which are used in these predictive codes and have not been previously measured for micron and sub-micron sized particles. Recent calculations have shown that particle size can significantly alter these coefficients from the values measured for bulk samples of a given material [27,28]. It is also important to compare experimentally measured charging characteristics of known particles in known plasmas in order to validate the various charging models that have been developed over the years.

In this program a technique and experimental system have been developed to measure secondary electron emission from sub-micron particles in free space. These represent the first reported measurement of secondary emission from sub-micron particles. Size effects produce substantial enhancements of secondary yield and in general corroborate the theoretical predictions of others.[27,28]

II. EXPERIMENT

The overall goal of this experimental program is to determine the effect that particle size has on the electron emission characteristics of micron and sub-micron grains. Differences from bulk values are expected because of geometrical considerations, electron penetration effects and possible electric field enhancement effects. To this end an experimental system was assembled to produce suitable dust grains, introduce them into a vacuum environment and diagnose their interaction with an electron beam.

Two different methods were used to produce particles for introduction into the vacuum system. The first is based upon work done by Sheehan and Carillo to break up agglomerations of prepared powders.[29] The device used is shown in Fig. 1 and consists of two cylindrical chambers separated by a fine mesh. Each chamber contains copper bb's coated with fibers which are used to break up the powders as the entire structure is shaken. This "duster" is placed in a

moderate pressure chamber (25 to 100 Torr) and vibrated at 30 to 60 Hz to produce a cloud of particles in the background flow of argon. Various materials were used including .01 to 1.0 μm alumina, 0.5 μm tungsten and 0.05 μm carbon. Although some data was generated, the duster proved problematic in that the powders would compact and the flow of particles into the system would fluctuate rapidly at times.

In the second particle generator, bismuth is evaporated in an oven and, as the vapor rises into a cooled area it nucleates in an inert background of argon which flows through the system. (See Fig 2.) The nucleation and growth rate of the particles is controlled by varying the temperature of the oven to change the vapor pressure and varying the argon pressure to change the collision rate.[30] In general, higher pressures and temperatures produce denser clouds of larger particles.

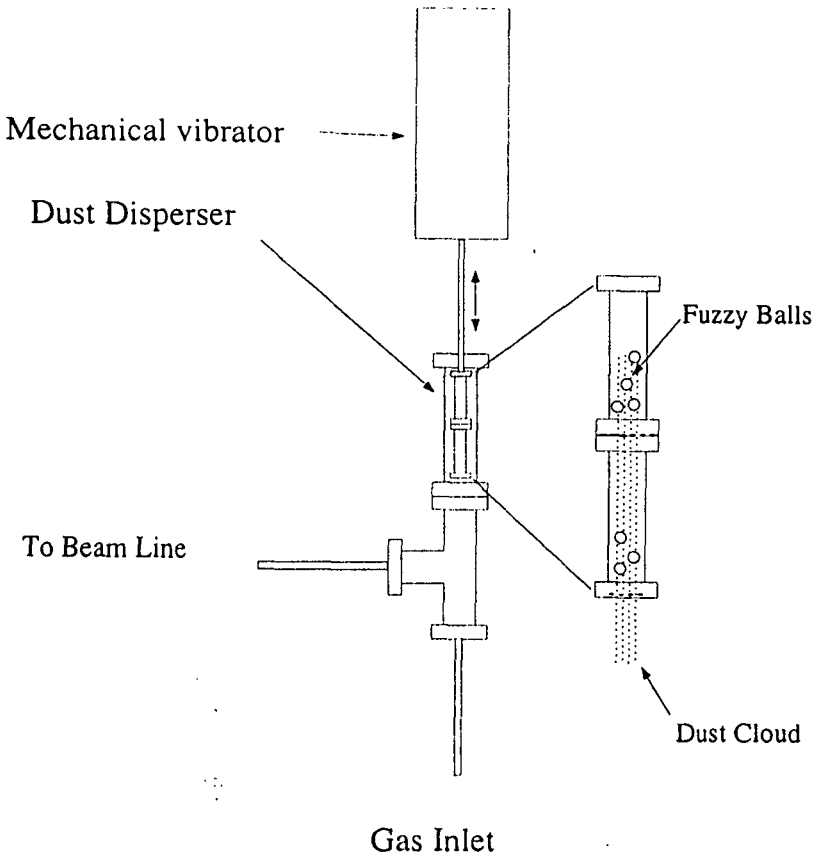

Figure 1. Vibrating duster used to introduce prepared powders into the experimental chamber.

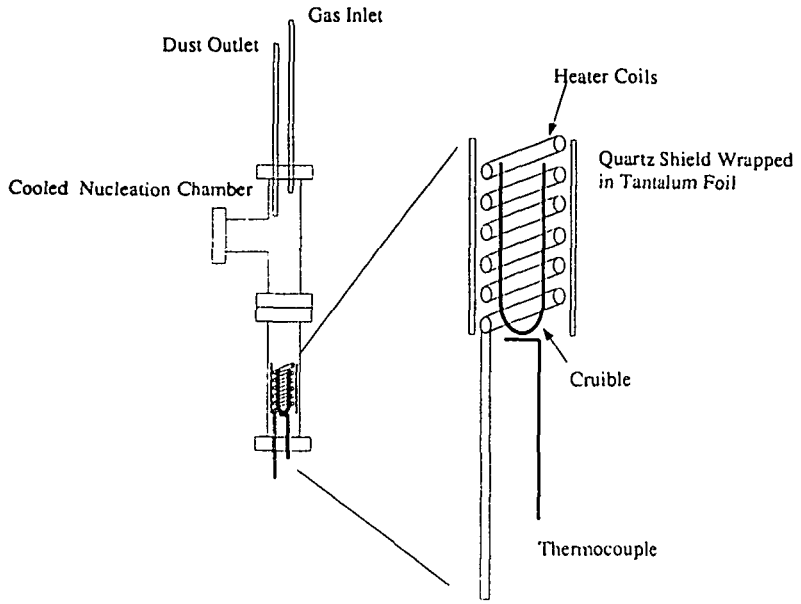

Figure 2. Oven system used to produce sub-micron bismuth particles and introduce them into the experimental chamber.

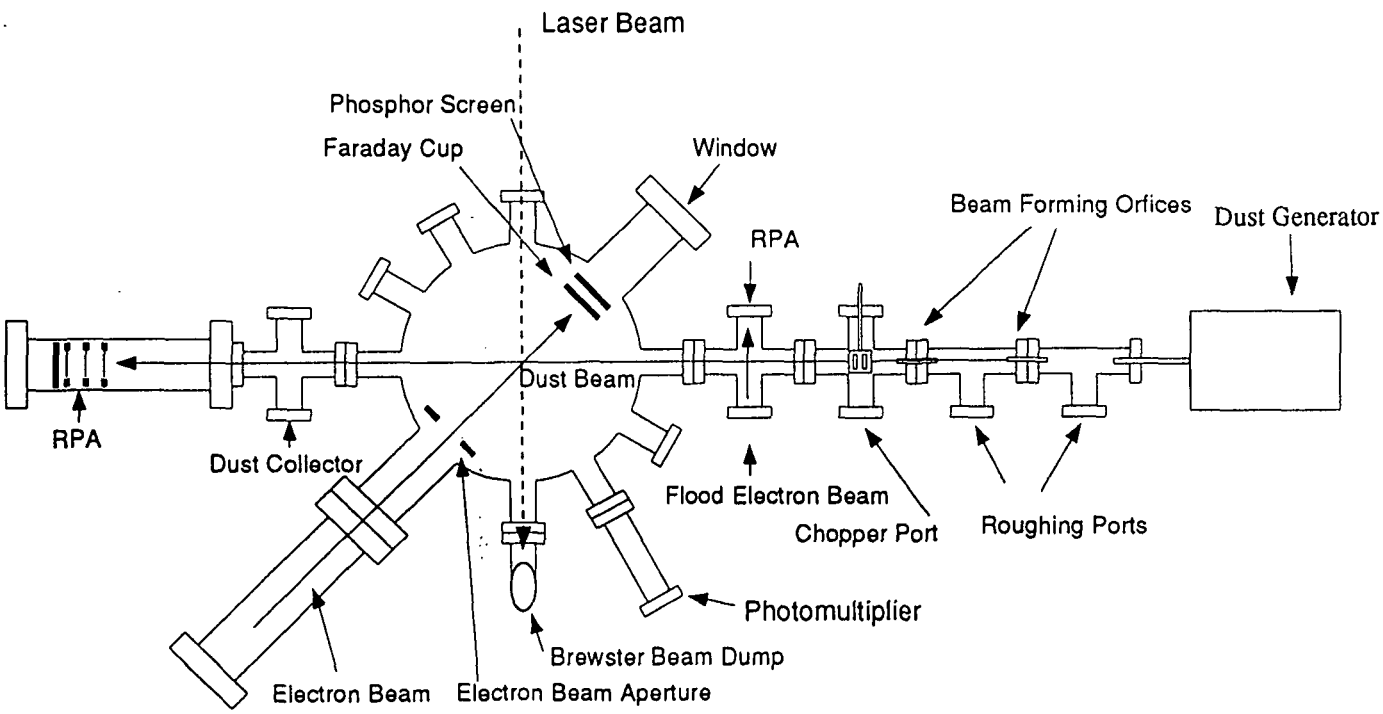

Figure 3. Experimental system used to measure secondary electron emission yield profiles.

The experimental layout is shown in Fig. 3. To the far right is the dust generator. The argon that flows through the system entrains the particles and transports them through a small tube to the experimental chamber. Because the electron beam must be operated in a high vacuum, the dust stream passes through a series of differentially pumped chambers which gradually strip the background gas while maintaining the flow of particles.

Once in the high vacuum region (still in the side arm), the dust beam first passes through a mechanical chopper which can produce pulses of dust particles at frequencies up to 90 Hz. Another chopper external to the arm cuts across the path of a LED/photodiode pair to produce an electrical signal at the same frequency as the dust beam. This signal can be used as the reference for lock-in amplifiers which can measure any small signals associated with the dust beam.

The dust beam then passes through a cross with a low energy electron beam (25-200 eV) which can be used to pre-charge the dust beam or provide a secondary emission reference. Directly across from this beam is a Faraday cup to monitor the electron current.

At the end of this arm the beam of dust particles streams across a multi-port vacuum chamber where a number of diagnostics and interactions can be applied to the dust beam. A laser scattering system is used to measure the average particle velocity, the radial density profile of the dust beam and to a lesser extent the relative size distribution of the grains in the beam. Figure 5 shows the results of scanning the laser beam across the dust to get a radial density profile. The dust beam is well defined and has a diameter of 2.5 mm

A high energy electron beam which has an energy range from 450 to 20,000 eV with a peak current density of 90 $\mu A/cm^2$ is mounted on a side arm of the main chamber. Its energy can be swept and a monitor signal is available to record the energy. Across the chamber from the gun are a phosphor screen and a Faraday cup used to monitor the beam position and current respectively. There is a 1.5 cm diameter aperture in the beam path prior to the dust/e-beam interaction region which crops the e-beam and maintains a well defined interaction length. A curved plate energy analyzer was placed across from the electron beam to calibrate the beam energy as a function of the e-beam power supply monitor voltage. Figure 4 shows the peak of a number of the energy spectra plotted against the monitor voltage and shows a linear correlation.

Just as the dust beam exits the main chamber it enters a small cross that houses a beam sampling apparatus. (See Fig.6) This apparatus consists of a mount that holds six sample grids for a transmission electron microscope (TEM) which can be moved into and out of the beam path. When out of the path the sample mount is hermetically sealed to prevent any contamination by dust accumulated in the main chamber. The dust collector is then back filled with filtered air. In this way extraneous particles are kept to a minimum.

In the center of the chamber a small (3mm) metal disk is mounted on a rod fed through the top of the chamber. This disk is used to align the various beams. It is first positioned in the center of the dust beam (measured by minimizing the current collected by the RPA). The e-beam is then translated until the shadow of the disk is centered in the electron beam. Finally the laser beam is centered on the disk. After this alignment the disk is retracted and measurements can be made.

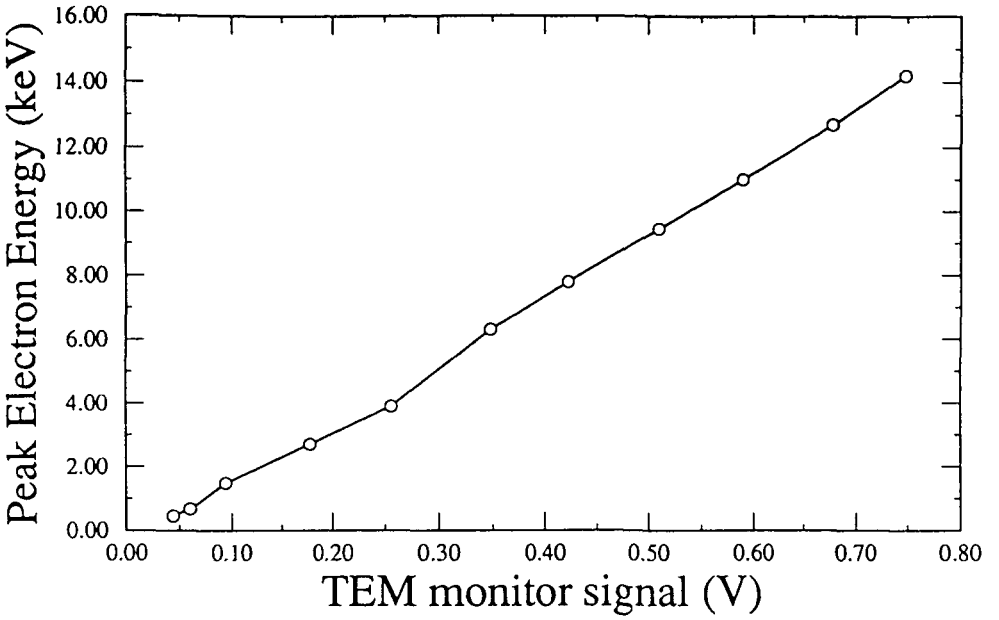

Figure 4. Calibration curve for the high energy electron beam monitor voltage made using a curved-plate electron energy analyzer.

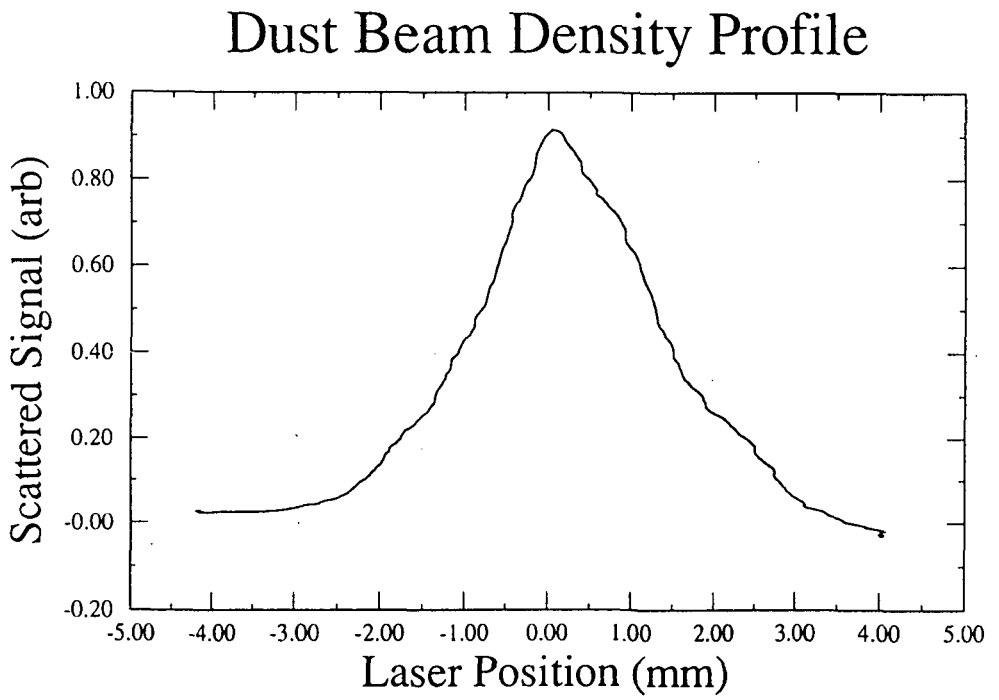

Figure 5. Laser scan of dust beam particle density profile.

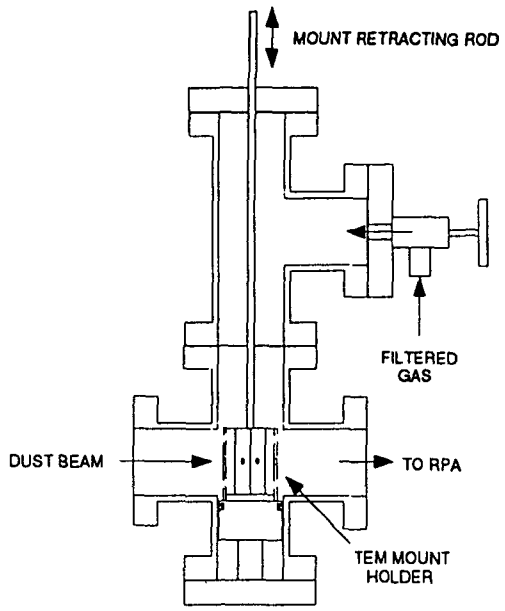

Figure 6. Sampling system used to collect dust particles for TEM analysis.

III. MEASUREMENTS

A secondary emission measurement is made for bismuth particles by first establishing a dust beam crossing the chamber. The particles are produced with an intrinsic negative charge, which , while the cause has not been determined, is convenient for the experiment. The oven is stabilized at a fixed temperature and pressure and the dust beam current, $I_{RPA,}$ is monitored using a Keithley model 480 picoammeter. The electron beam is centered on the dust beam and the beam energy is swept and digitally recorded along with I_{RPA} and the electron beam current, I_{FC} (which varies with e-beam energy). The relative change of the dust current, ΔI_{RPA}, is proportional to the secondary electron emission coefficient, δ. For $\delta > 1$, I_{RPA} reduces as the particles are discharged and for $\delta < 1$ I_{RPA} increases as charge is added. Figure 7 shows a data set with I_{RPA}, I_{FC}, and $\Delta I_{RPA}/I_{FC}$ displayed as a function of beam energy.

Equations 1 and 2 define the change in the RPA collector current due to the effects of the high energy and low energy electron beams. The change is a function of the incident current density, J, the total cross section of the particles, n_{part} σ_{part}, and the total time the particle is each beam, $v_{part}l$. The ratio of these equations eliminate v_{part}, n_{part}, and σ_{part} and can be rearranged to give δ as a function of readily available parameters. In order to calibrate this curve, δ must be

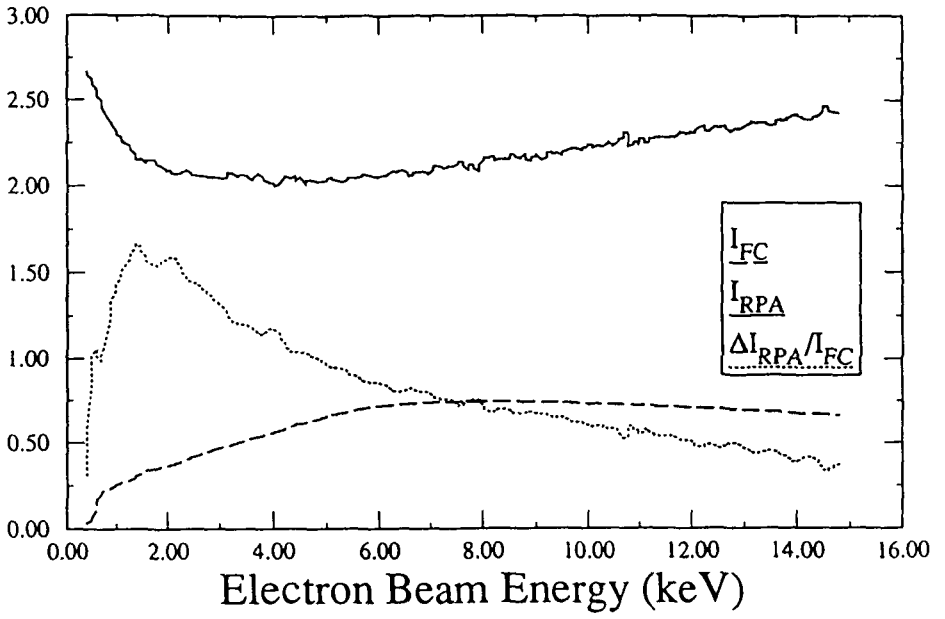

Figure 7. Experimental data showing the collected dust beam current, I_{RPA}, the incident electron beam current, I_{FC}, and the change in dust beam current normalized to the electron beam current, $\Delta I_{RPA}/I_{FC}$ as a function of electron energy. Using from the low energy electron beam the last curve is then converted into an absolute yield profile.

known accurately at some energy. This is the role of the low energy e-beam. The penetration depth of a 25 eV electron is 0.1 nm, far less than the size of any of the particles measured herein. Therefore effects due to electron penetration are not important. Shih and Hor have recently show theoretically and experimentally that the angle of incidence of the electron has no noticeable effect on δ for energies less than 50 eV [30]. Therefore, at 25 eV, δ is the same for the particle and bulk materials. Based on published data for bismuth, δ(25 eV) = 0.214 [30]. With this known value at 25 eV, the response of the dust beam current to the low energy electron beam at a fixed current density can be used to normalize the high energy data and derive absolute secondary emission curves.(eq. 3)

$$\Delta I_{RPA}(\epsilon) = J_{HEB}\,\sigma_{part}\,[\delta(\epsilon)-1]\,n_{part}\,v_{part}\,l_{HEB} \tag{1}$$

$$\Delta I_{RPA}(25eV) = J_{LEB}\,\sigma_{part}\,[\delta(25eV)-1]\,n_{part}\,v_{part}\,l_{LEB} \tag{2}$$

$$\delta(\epsilon) = 1 + \frac{J_{LEB} l_{LEB} [\delta(25eV) - 1] \Delta I_{RPA}(\epsilon)}{J_{HEB} l_{HEB} \Delta I_{RPA}(25eV)} \quad (3)$$

A series of measurements were made in which the oven parameters were set, two secondary scans made and a dust sample collected. Figure 8 shows a TEM photograph of a collection of particles. They are quite spherical and exhibit a range of sizes. Figure 9 shows the particle size distributions derived from similar photos for three different oven conditions. The mean diameter ranges from 22 to 80 nm while the half-width decreases for the smaller particles. Figure 10 shows the secondary emission curves for these three distributions. The effects of size are dramatic, especially when compared to the curve for bulk bismuth. also shown. For the smallest particle δ_{max} = 4.5 compared with the bulk value of 1.2.[31]

Figure 8. TEM photograph of bismuth particles collected resulting in a size distribution of d = 22 ±12 nm.

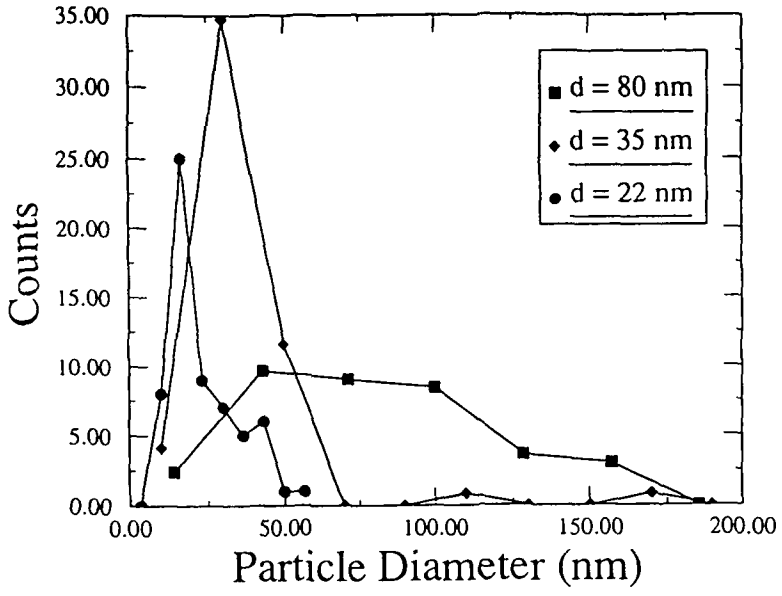

Figure 9. Particles size distribution derived from TEM photos for three different bismuth oven conditions.

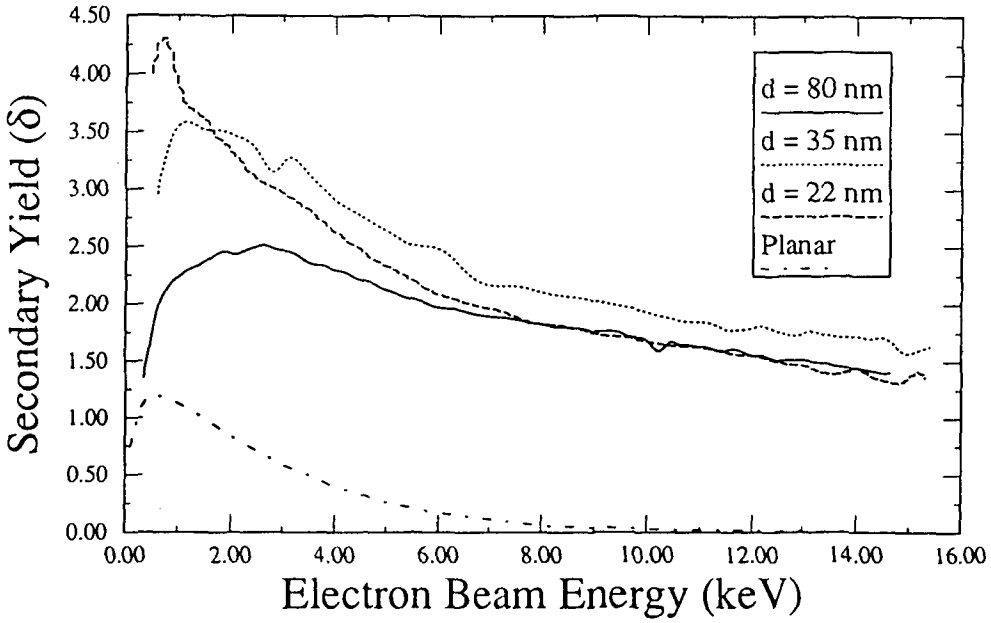

Figure 10. Secondary emission yields corresponding to the size distributions of Fig. 4.

Similar measurements were attempted with prepared powders. In this case the flux of particles was less, and lock-in amplifiers were used. The magnitude of the flux was very inconsistent, and therefore a method was devised to normalize the current collected by the RPA. The scattered laser light signal was recorded at the same time as the RPA current. Assuming that the shape of the particle size distribution remains relatively constant as the total flux varies, the magnitude of the laser signal is representative of the particle density. Therefore, dividing the RPA signal by the laser signal should produce a smooth curve. Figure 11 shows an example of data taken while sweeping the retarding grid on the RPA. While the two raw signals vary greatly, the normalized curve was reasonably smooth and exhibited the shape expected (the number of charged particles reaching the collector monotonically decreases as the absolute value of the retarding potential increases). In previous studies such curves were analyzed to determine the size distribution of fully charged particles.[25] Although, such short term measurements could be made, measurements of the secondary emission were too inconsistent to be useful.

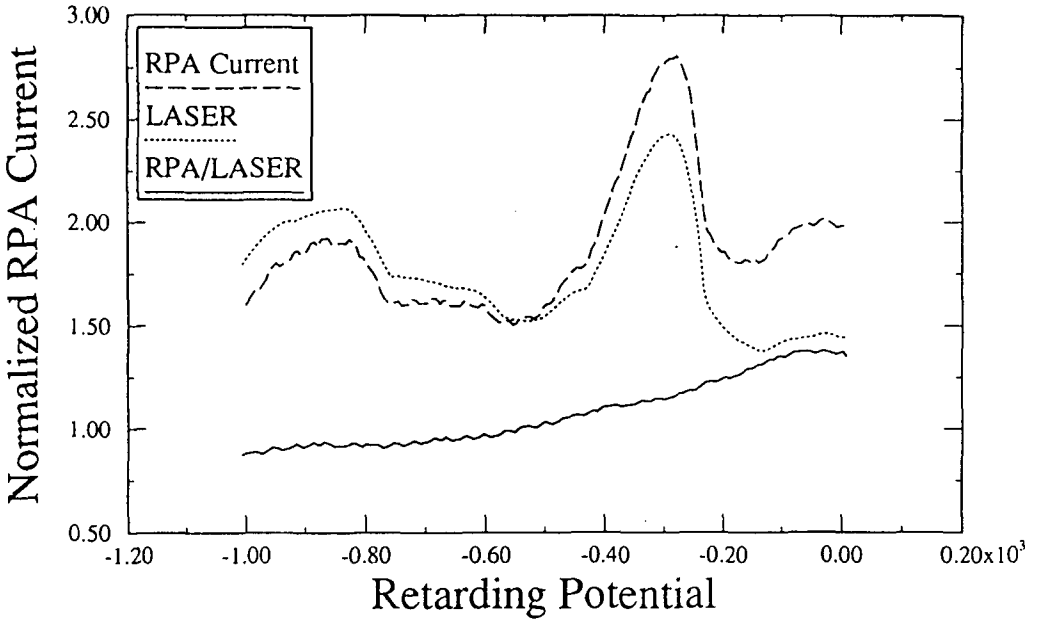

Figure 11. RPA current and laser scattered signal acquired with lock-in amplifiers during a sweep of the retarding grid for a dust beam generated from prepared powders. Note that the normalized signal shows a proper profile for such a sweep.

IV. DISCUSSION OF RESULTS

These results represent the first experimental measurement of the effect of particle size on the secondary emission yield of a material. Only recently has there been any theoretical studies carried out on the subject. In two papers, Chow et al. have addressed the effects of size [27, 28] In the first, $\delta(\varepsilon)$ is calculated for micron and sub-micron metal and dielectric particles assuming that particles immersed in a plasma will experience an electron flux that is everywhere normal to the surface. (See Fig. 12a) Figure 13 shows their results for generic metallic and dielectric particles. In comparing with the data in Fig 10 one can see a close correlation at lower energies. However at higher energies the measured δ's are substantially higher. This is likely due to angular effects which are addressed in Chow et al.'s second paper where the electrons are postulated to be the form of a mono-energetic, collimated beam, similar to our experimental configuration. (see Fig. 12b) In this case calculations were done for a dielectric particle 1.12 μm in diameter.(See Fig. 14) Although only one size was studied, one can see that the yield remains greater than on for all energies as we have seen experimentally.

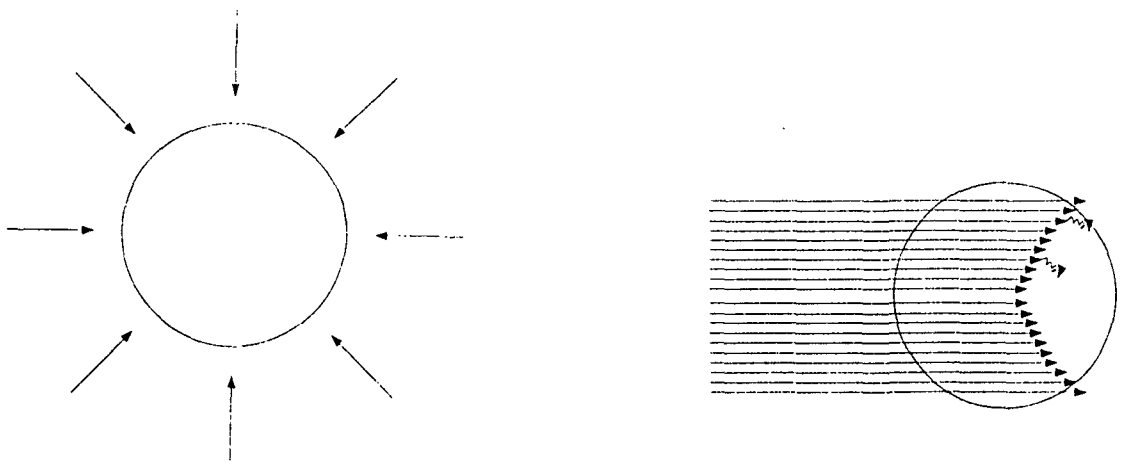

a) b)

Figure 12. Schematics of the electron impact for a particle immersed a). in a plasma and b). in a collimated electron beam.

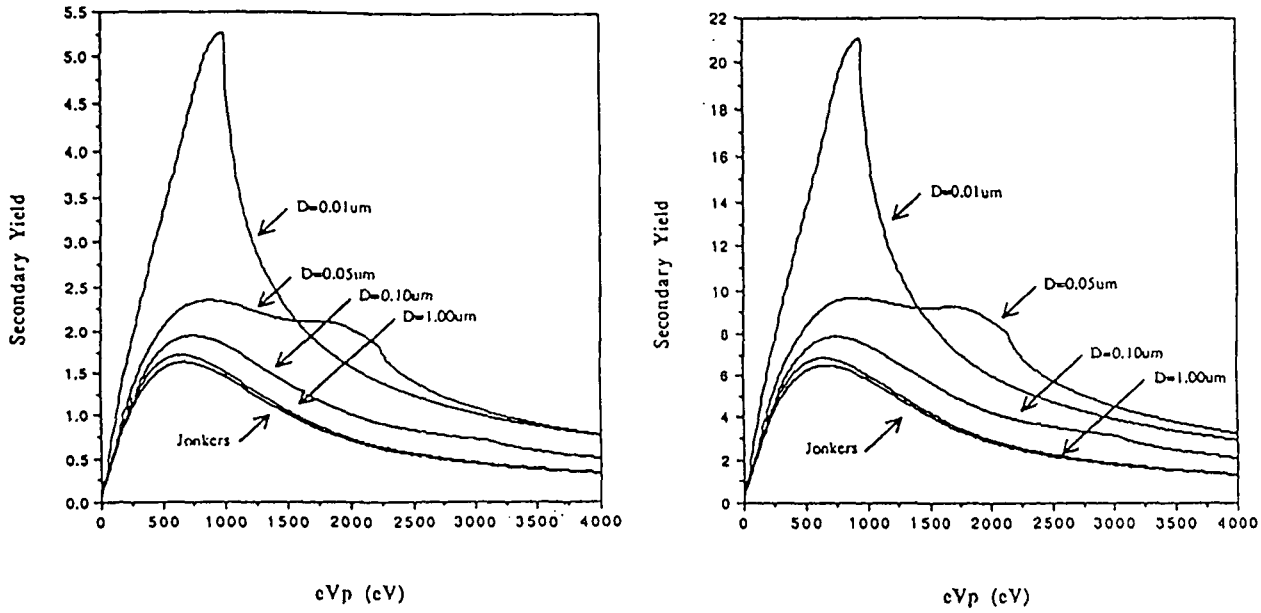

Figure 13. Theoretically predicted secondary emission profiles for metal (a) and dielectric spheres. Calculations were made assuming that the electrons are everywhere normal to the particle surface.(After Chow et al.[27])

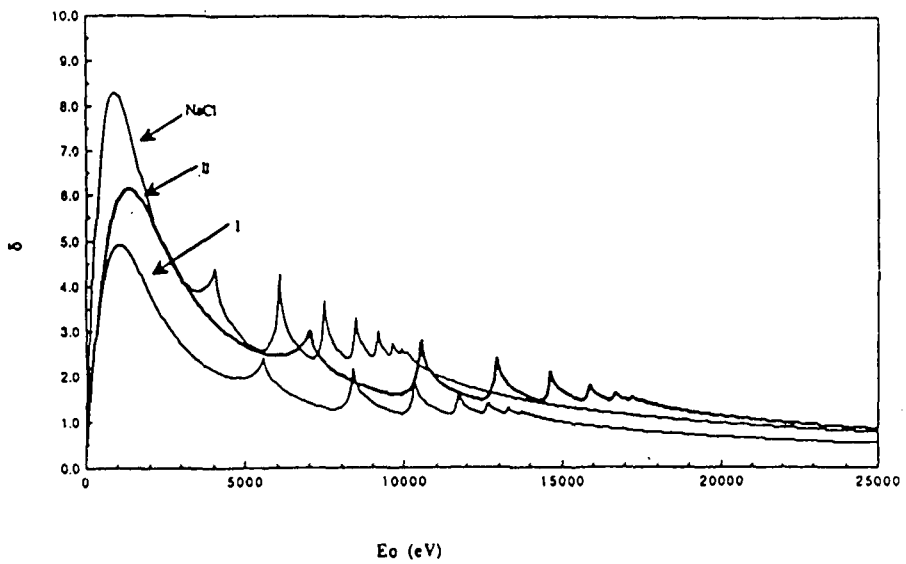

Figure 14. Theoretically predicted secondary emission yield profiles for dielectric spheres with d = 1.12 μm made assuming a collimated electron beam. Curves I and II are for a glass sphere with different assumed values of secondary electron escape depths and electron excitation energies (After Chow et al. [28]).

This is a consequence of the fact that the electrons are penetrating the particles. Figure 15 shows the mean range of electrons in metal and dielectric materials calculated using Whiddington's law. For our maximum energies the mean ranges are much greater than the diameter of the particles. If no energy is deposited, one electron leaves for every electron that hits the surface giving an effective minimum delta of 1. Although the electron are fully penetrating, they still deposit a portion of their energy giving rise to additional emission.

This is different from bulk materials, where δ continues to drop toward a value normally in the range of $\delta = 0.1$. This minimum is representative of electron backscatter rather then true secondary emission. The ramification is that small particles are essentially transparent to high energy electrons and these electrons will consequently have little impact upon the charging of the particle.

For an initially neutral bismuth particle, a flux of electrons with an energy greater than 400 eV would cause the particle to charge positively. If all secondary electrons created could escape, the particle would acquire a positive potential of several kilovolts. This will not happen because secondary electrons typically have energies of less than 100 eV, and hence charging would stop when the secondaries could no longer overcome the grain potential. This of course presents more problems for modelers since the charging is now dependent upon the details of the energy spectra of the secondary electrons.

Another significant feature is the sensitivity of yields for identical glass spheres (curves I and II) to the assumed values of secondary electron escape depth and electron excitation energies. This demonstrates the continued need for experimental studies to provide basic parameters for modelers and to validate the subsequent theoretical predictions.

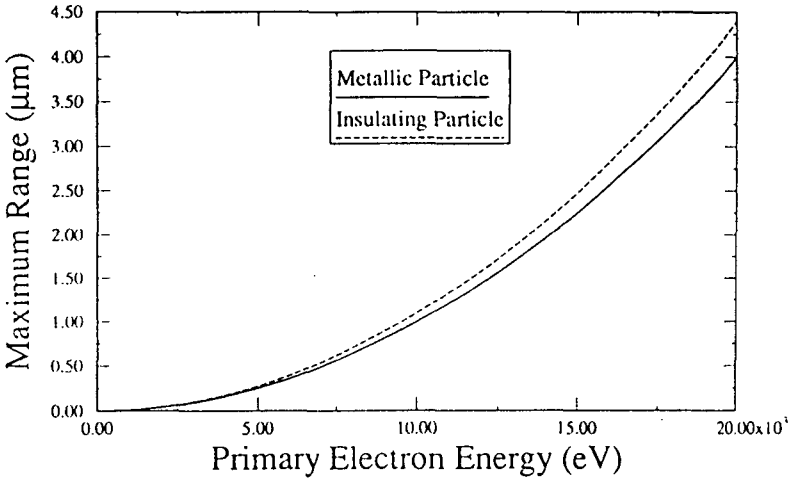

Figure 15. Electron mean ranges for typical metal and dielectric parameters calculated using Whiddington's law.

V. CONCLUSIONS

An experimental system has been developed to measure the secondary emission from sub-micron particles in free space without any interference from any support structure.

Using this system the first such measurements have been made. It has been experimentally demonstrated that size has a substantial influence on the secondary emission profile of sub-micron particles. These measured profiles are in general accord with theoretical predictions.

VI. FUTURE WORK

The measurements were made for ensembles of particles with fairly broad size distributions. Therefore methods to narrow the size distribution should be implemented and measurements should be repeated to further quantify the effects of size.

Since the secondary emission varies widely for different materials, measurements should be made for other materials such as silicates and carbon compounds which are postulated to exist in various space environments.

After secondary emission, photo emission has the greatest influence upon the equilibrium charge of a particle.[32] The experimental system is equally well suited to the study of the interaction of uv radiation with the sub-micron particles.

Because of their small size the acquisition of modest charge levels can produce very large local electric fields.[33,34] Again the experimental system is uniquely suited to the measurement of field enhanced secondary and photo emission.

REFERENCES

[1] A.Z. Dolginov, V.S. Kessel'man, and M.B. Parizh, *Sticking and Growth of Oppositely Charged Dust Grains in Protostellar Clouds*, Sov. Astron. **27**, 655 (1983).

[2] H. Mizuno, W.J. Markiewiez, and H.J. Völk, *Grain Growth in Turbulent Protoplanetary Accretion Disks,* Astron. Astrophys. **195**, 183 (1988).

[3] G.R. Gisler and E.R. Wollman, *Grain Plasma, Simulations of Electrically Polarized Gravitational Condensation*, Phys. Fluids **31**, 1101 (1988).

[4] C.K. Goertz and Linhua-Shan, *Electrostatics Forces in Planetary Rings*, Geophys. Research Lett. **15**, 84 (1988).

[5] T.G. Northrop, D.A. Mendis, and L. Schaffer, *Gyrophase Drifts and the Orbital Evolution of Dust at Jupiter's Gossamer Ring*, Icarus **79**, 101 (1989).

[6] Lin-Hua Shan and C.K. Goertz, *On the Radial Structure of Saturn's B Ring*, The Astrophys. J. **367**, 350 (1991).

[7] D.A. Mendis, H.L.F. Houpis, and J.R. Hill, *The Gravito-Electrodynamics of Charged dust in Planetary Magnetospheres*, J. of Geophys. Research **87**, 3449 (1982).

[8] C.K. Goertz, *Dusty Plasmas in the Solar System*, Reviews of Geophys. **27**, 271 (1989).

[9] O. Havnes, *A Streaming Instability Interaction Between the Solar Wind and Cometary Dust*, Astron. Astrophys. **193**, 309 (1988).

[10] F. Hoyle and N.C. Wickramasinghe, *Interstellar Extinction by Cometary Organic Grain Clumps*, Astrophys. and Space Sci. **140**, 191 (1988).

[11] O.L. Vaisberg, V.N. Smirnov, L.S. Gorn, M.V. Iovlev, M.A. Balikchin, S.I.Klimov, S.P. Savin, V.D. Shapiro, and V.I. Shevchenko, *Dust Coma Structure of Comet Halley from SP-1 Detector Measurements*, Nature **321** ,274 (1986).

[12] J.R. Fincke, W.D. Swank, and C.L. Jeffery, *Simultaneous Measurement of Particle Size, Velocity, and Temperature in Thermal Plasmas*, IEEE Trans. Plas. Sci. **18**, 948, (1990).

[13] G.S. Selwyn, J.E. Heindenreich and K.L. Haller, *Particle Trapping Phenomena in Radio Frequency Plasmas*, Appl. Phys. Lett. **57**, 1876 (1990).

[14] R.P. Donovan, ed., **Particle Control for Semiconductor Manufacturing** (Marcel Dekker, NY, 1990).

[15] R.A. Bowling, G.B. Larrabee and W.G. Fisher, *Status and Needs of In-Situ Real-Time Process Particle Detection*, J. Env. Sci., (Sept./Oct. 1989).

[16] G.S. Selwyn, *Plasma Particulate Contamination Control. I. Transport and Process Effects*, J. Vac. Sci. Technol. **B9**, 3487 (1991).

[17] B.D. Moyle and J.F. Hughes, *Corona Charging of Insulating Particles*, Inst. Phys. Conf. No. **66**: Session VI, 155 (1983).

[18] H.A. Bridgman, *Measured and Theoretical Particle Size Distribution Over Industrial and Rural Locations at Milwaukee April 1976*, Atmospheric Environment **13**, 629 (1979).

[19] K. Tedjojuwono, Y. Kawase, and T. Asakura, *Studies of the Dynamic Behavior of Charged Dust Particles in High Electric Fields using Laser Doppler Velocimetry,* Optics and Laser Technology, 187 (1981).

[20] N. Meyer-Vernet, *"Flip-Flop" of Electric Potential of Dust Grains in Space*, Astron. Atrophys. **105**, 98 (1982).

[21] O. Havnes, C.K. Goertz, G.E. Morfill, E. Grün, and W. Ip, *Dust Charges, Cloud Potential, and Instabilities in a Dust Cloud Embedded in a Plasma*, J. Geophys. research **92**, 2281 (1987).

[22] D.A. Mendis, *The Role of Field Emission in the Electrostatic Disruption of Cosmic Dust*, Astrophys. and Space Sci. **176**, 163 (1991).

[23] F. Melandso, T.K. Aslakaen, and O. Havnes, *A KInetic Model for Dust Acoustic Waves Applied to Planetary Rings*, J. Geophys. Res., **98**, 13,315 (1993).

[24] B. Young, T.E. Cravens, T.P. Armstrong, and R.J. Friauf, *A Two-dimensional Particle-in-Cell Model of a Dusty Plasma*, J. Geophys. Res., **99**, 2255 (1994).

[25] R.C. Hazelton and E.J. Yadlowsky, *Measurement of Dust Grain Charging in a Laboratory Plasma*, IEEE Trans. Plas. Sci., **22**, 91, (1994)

[26] B. Walch, M. Horanyi, and S. Robertson, *measurement of the Charging of Individual Dust Grains in a Plasma*, IEEE Trans. Plas. Sci., **22**, 97, (1994).

[27] V.W. Chow, D.A. Mendis, and M. Rosenberg, *The Role of Grain Size and Particle Velocity Distributions in Secondary Electron Emission in Space Plasmas,* J. Geophys. Res., **98**, 19,065, (1993).

[28] V.W. Chow, D.A. Mendis, and M. Rosenberg, *Secondary Emission from Small Dust Grains at High Electron Energies*, IEEE Trans. Plas. Sci., **22**, 179, (1994).

[29] D.P. Sheehan and M. Carillo, *Device for Dispersal of Micrometer and Submicrometer-sized Particles in Vacuum,* Rev. Sci. Instrum., **61**, 3871 (1990)

[30] A. Shih and C. Hor, *Secondary Emission Properties as a Function of the Electron Incidence Angle*, IEEE Trans. Electr. Dev., **40**, 824, (1993).

[31] CRC Handbook of Chemistry and Physics, R.C. Weast, ed., CRC Press, Boca Raton, Fl., (1986).

[32] B. Feuerbacher and B. Fitton, *Experimental Investigation of Photoemission From Satellite Surface Materials,* J. App. Phys., **43**, 1563 (1972).

[33] C. Yunming and L. Ming, *A New Model for the Floating Potential of Fine Particles in Plasma*, J. Phys. D, **26**, 1007 (1993).

[34] E.J. Yadlowsky and R.C. Hazelton, *Effect of a Nonpenetrating Electron Beam on Enhancing Photoelectron Yield,* J. Appl. Phys., **75**, 3619 (1994).